



Redox-Active Carbohydrate-Coated Nanoparticles: Self-Assembly of a Cyclodextrin–Polystyrene Glycopolymer with Tetrazine–Naphthalimide

Andrew Gross, Raoudha Haddad, Christophe Travelet, Eric Reynaud, Pierre Audebert, Redouane Borsali, Serge Cosnier

► To cite this version:

Andrew Gross, Raoudha Haddad, Christophe Travelet, Eric Reynaud, Pierre Audebert, et al.. Redox-Active Carbohydrate-Coated Nanoparticles: Self-Assembly of a Cyclodextrin–Polystyrene Glycopolymer with Tetrazine–Naphthalimide. *Langmuir*, 2016, 32 (45), pp.11939 - 11945. 10.1021/acs.langmuir.6b03512 . hal-01644738

HAL Id: hal-01644738

<https://hal.science/hal-01644738>

Submitted on 19 Nov 2020

HAL is a multi-disciplinary open access archive for the deposit and dissemination of scientific research documents, whether they are published or not. The documents may come from teaching and research institutions in France or abroad, or from public or private research centers.

L'archive ouverte pluridisciplinaire **HAL**, est destinée au dépôt et à la diffusion de documents scientifiques de niveau recherche, publiés ou non, émanant des établissements d'enseignement et de recherche français ou étrangers, des laboratoires publics ou privés.


1 Redox-Active Carbohydrate-Coated Nanoparticles: Self-Assembly of 2 a Cyclodextrin–Polystyrene Glycopolymer with Tetrazine– 3 Naphthalimide

4 Andrew J. Gross,[†] Raoudha Haddad,[†] Christophe Travelet,^{‡,§} Eric Reynaud,^{‡,§} Pierre Audebert,^{||}
5 Redouane Borsali,^{*,‡,§} and Serge Cosnier^{*,†}

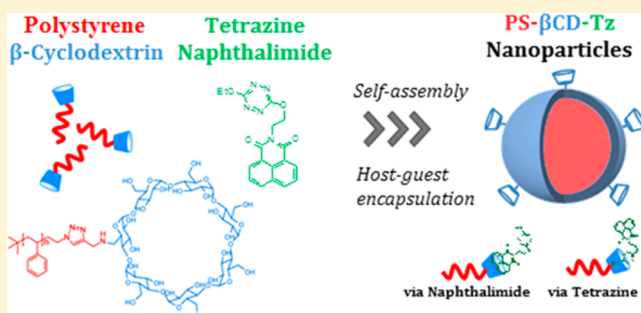
6 [†]Department of Molecular Chemistry, CNRS UMR 5250 and [‡]CERMAV, Université Grenoble Alpes, 38000 Grenoble, France

7 [§]CNRS, CERMAV, 38000 Grenoble, France

8 ^{||}PPSM, CNRS UMR 8531, ENS Cachan, 61 Avenue du Président Wilson, 94235 Cachan, France

9  Supporting Information

10 **ABSTRACT:** The controlled self-assembly of precise and
11 well-defined photochemically and electrochemically active
12 carbohydrate-coated nanoparticles offers the exciting prospect
13 of biocompatible catalysts for energy storage/conversion and
14 biolabeling applications. Here an aqueous nanoparticle system
15 has been developed with a versatile outer layer for host–guest
16 molecule encapsulation via β -cyclodextrin inclusion complexes.
17 A β -cyclodextrin-modified polystyrene polymer was first
18 obtained by copper nanopowder click chemistry. The
19 glycopolymer enables self-assembly and controlled encapsula-
20 tion of tetrazine-naphthalimide, as a model redox-active agent,
21 into nanoparticles via nanoprecipitation. Cyclodextrin host–
22 guest interactions permit encapsulation and internanoparticle cross-linking for the formation of fluorescent compounds and
23 clustered self-assemblies with chemically reversible electroactivity in aqueous solution. Light scattering experiments revealed
24 stable particles with hydrodynamic diameters of 138 and 654 nm for nanoparticles prepared with tetrazine, of which 95% of the
25 nanoparticles represent the smaller objects by number. Dynamic light scattering revealed differences as a function of preparation
26 method in terms of size, 3-month stability, polydispersity, radius of gyration, and shape factor. Individual self-assemblies were
27 visualized by atomic force microscopy and fluorescence microscopy and monitored in real-time by nanoparticle tracking analysis.
28 UV–vis and fluorescence spectra provided insight into the optical properties and critical evidence for host–guest encapsulation
29 as evidenced by solvachromatism and enhanced tetrazine uptake. Cyclic voltammetry was used to investigate the electrochemical
30 properties and provided further support for encapsulation and an estimate of the tetrazine loading capacity in tandem with light
31 scattering data.



32 ■ INTRODUCTION

33 The development of biocompatible nanoassembled particles
34 with controlled chemical and physical properties has attracted
35 significant attention for applications such as imaging,
36 biosensing, drug delivery, and biocatalysis.^{1,2} Nanoparticles
37 such as micelles capable of carrying and delivering redox
38 molecules in a selective manner have shown great benefits
39 including enhanced bioavailability,³ stimuli-responsiveness,⁴
40 and reduced toxicity.⁵ However, polymer synthesis and particle
41 assembly methods are often complicated and time-consuming.⁶
42 Furthermore, challenges remain for in vivo and in vitro
43 applications including solubility and stability issues.

44 The preparation of amphiphilic glycopolymers provides a
45 route to biocompatible and bioinspired nanoparticles but
46 remains relatively undeveloped because of their tricky
47 preparation with many synthesis steps.^{7–9} Several groups
48 have now reported on the preparation and self-assembly of
49 block copolymers containing polysaccharides and oligosacchar-

ides (maltoheptaose,¹⁰ dextrans,^{9,11} and amylose¹² with
synthetic polymers such as polystyrenes,^{9–13} poly(ϵ -
caprolactone)s,¹⁴ poly(ethylene glycol)s¹⁵ and poly(methyl
methacrylate)s¹⁶). Amphiphilic block copolymer formation is
generally achieved using combinations of controlled living
radical polymerizations, transition-metal-mediated coupling
chemistry, and tedious purification procedures.⁷ Many methods
report the self-assembly of amphiphilic block copolymers into
nanoparticles by direct dissolution into a selective solvent for
one of the block moieties.^{9,11,17,18} However, with this approach
it is difficult to avoid random aggregation and control particle
size at the nanoscale. Clever manipulation strategies involving
indirect dissolution methods such as nanoprecipitation facilitate
the preparation of well-defined micellar nanoparticles with

Received: September 25, 2016

Revised: October 20, 2016

Published: October 25, 2016



64 narrow polydispersities from water or mixed solvent–water
65 copolymer solutions.^{13,16,19} Nanoprecipitation, first reported by
66 Fessi and co-workers, involves the dissolution of both blocks
67 followed by precipitation and selective solvent removal.^{20,21} A
68 further advantage is that redox molecules or drugs can be
69 dissolved in copolymer solution prior to precipitation. In this
70 case, hydrophobic species can be trapped as cargo inside the
71 dense hydrophobic core of nanoassembled particles.^{10,22}

72 A more sophisticated approach to encapsulation is to
73 incorporate chemical handles capable not only of trapping
74 but also of orienting and stimuli-controlled releasing of redox
75 molecules in aqueous solution.²³ Methods capable of molecule
76 encapsulation in the outer layer may further benefit from
77 improved redox molecule bioavailability and accessibility.
78 Cyclodextrins are one class of functional molecules capable of
79 selectively binding a vast array of compounds via host–guest
80 interactions.^{24–27} Their low solubility in water leads to
81 spontaneous aggregation, but functionalized cyclodextrins
82 with carefully designed polymer blocks have been used to
83 prepare nanoassembled particles.^{7,9,13}

84 In this article, we describe a new straightforward synthesis
85 route for the synthesis of a β -cyclodextrin-modified polystyrene
86 polymer (PS-CD) and its use in the self-assembly of redox-
87 active nanoparticles in water via encapsulation of a model
88 hydrophobic molecule, tetrazine-naphthalimide (Tz). This
89 molecule was recently developed by us and is of interest for
90 future applications in fluorescence sensing and labeling.^{28,29}

91 The PS-CD glycopolymer was synthesized according to a
92 simple procedure that uses a copper nanopowder catalyst rather
93 than copper in solution to covalently couple functionalized β -
94 cyclodextrin and polystyrene blocks via click chemistry with a
95 high yield of 90%. (See the [Supporting Information](#) for
96 synthesis and characterization details.) We previously used CuI
97 to couple β -cyclodextrin and PS groups, but the Cu in solution
98 was difficult to remove so it was not possible to synthesize a
99 large amount of clean glycopolymer.¹³ In contrast, the Cu
100 nanopowder employed here is very easy to remove via classical
101 filtration and CupriSorb resin, facilitating preparation and
102 purification of the modified polymer on a larger scale.

103 ■ EXPERIMENTAL SECTION

104 **General Materials and Apparatus.** The ω -hydroxy-polystyrene
105 ($M_n = 3800 \text{ g mol}^{-1}$) was purchased from Polymer Source. Tetrazine-
106 naphthalimide was synthesized according to our previously reported
107 work.²⁹ Propargylamine, sodium hydroxide (NaOH), tetrahydrofuran
108 (THF), *N,N*-dimethylformamide (DMF), sodium azide (NaN_3), and
109 diatomaceous earth were purchased from Sigma-Aldrich. β -Cyclo-
110 dextrin and Cu/CuO nanopowder were purchased from Alfa Aesar.
111 Tosyl chloride (TsCl) was obtained from Fluka, and pyridine was
112 purchased at SDS. Methanol (MeOH) and dichloromethane
113 (CH_2Cl_2) were purchased from Biosolve. Milli-Q water was obtained
114 by water purification to a resistivity of $18.2 \text{ M}\Omega \text{ cm}$ using a Millipore
115 Ultrapure system. Deuterated solvents were purchased from Euriso-
116 top, the Cuprisorb resin was purchased from Seachem, and the
117 Si(100) wafers were purchased from Siltronix. All reagents and
118 solvents used for the synthesis of tetrazine-naphthalimide were
119 purchased from Sigma-Aldrich or Carlo-Erba.

120 ^1H NMR spectra were recorded on a Bruker Avance 400 MHz
121 spectrometer with a frequency of 400.13 MHz and calibrated with the
122 deuterated solvent signal.³⁰ The analysis characteristics were $z\theta = 90^\circ$,
123 $D1 = 1 \text{ s}$, and $NS = 128$ scans. Matrix-assisted laser desorption
124 ionization time-of-flight mass spectrometry (MALDI-TOF-MS) was
125 performed using an Applied Biosystems Voyager-DE STR-H equipped
126 with a nitrogen laser (337 nm and 3 ns pulse width).

UV–vis absorption spectra were recorded in quartz cuvettes using a
PerkinElmer UV-Lambda 650 spectrophotometer, and fluorescence
spectra were recorded using a PerkinElmer LS50.

Synthesis of β -Cyclodextrin-Modified Polystyrene Polymer.
The amphiphilic glycopolymer was obtained by click chemistry. The
first step was to functionalize each block: the hydrophobic block, ω -
hydroxyl-terminated polystyrene, was functionalized to form ω -azido-
terminated polystyrene via the ω -tosyl terminated polystyrene
intermediate with an overall yield of 75% according to the method
of Fallais and co-workers.³¹ The hydrophilic block, native β -
cyclodextrin, was monofunctionalized into mono-6-alkyne- β -cyclo-
dextrin via the mono-6-tosyl- β -cyclodextrin intermediate with an
overall yield of 7% according to the procedure developed by
Moutard.^{32,33} Both blocks with their complementary chemical
functions (alkyne and azido) were subsequently linked together via a
click reaction in heterogeneous media catalyzed by Cu nano-
powder^{34,35} to obtain the β -cyclodextrin-modified polystyrene polymer
($M_n = 4900 \text{ g mol}^{-1}$, PDI = 1.01) (Scheme S1). To perform the click
reaction, a degassed solution containing the azido-functionalized
polystyrene (1 equiv, 8.1 g, $1.8 \times 10^{-3} \text{ mol}$) and the alkynyl-
functionalized cyclodextrin (1.2 equiv, 2.7 g, $2.2 \times 10^{-3} \text{ mol}$) in DMF
was first prepared. An excess of Cu nanopowder (1.8 equiv, 260 mg,
 $3.2 \times 10^{-3} \text{ mol}$) was added to the solution and the mixture stirred
under Ar at 65°C for several hours until the azide ^1H NMR signal
disappeared. At the end of the reaction, the crude heterogeneous
mixture was filtered off under diatomaceous earth, and the obtained
filtrate was stirred several hours in the presence of the Cuprisorb resin.
The mixture was finally precipitated in cold MeOH to give a white
powder with a yield of 90% (mass = 8 g). The modified polymer
structure was confirmed using NMR and MALDI analysis (Figure S1).

**Preparation of PS-CD_{NP} and PS-CD-Tz_{NP} Nanoparticles via
Nanoprecipitation.** Polymer solutions were prepared by dissolving
either 5 mg of PS-CD or 5 mg of PS-CD together with 1 mg of
tetrazine in 5 g of a THF/H₂O solution (80:20 v/v %, unless
otherwise stated). For nanoprecipitation by method A, 1 g of the PS-
CD solution was slowly added dropwise to 40 g of Milli-Q water under
stirring at 500 rpm at room temperature. For nanoprecipitation by
method B, 40 g of water was slowly added to 1 g of the PS-CD
solution under stirring at 500 rpm at room temperature. The solutions
were subsequently stirred at 500 rpm at room temperature for 1.5 h
and then preconcentrated to 4 g by evaporation under reduced
pressure at 50°C using a rotary evaporator. The nanoparticle
suspensions were stored at room temperature in the dark.

**Static Light Scattering (SLS)/Dynamic Light Scattering
(DLS).** Light scattering measurements were performed using an
ALV/CGS-8FS/N069 goniometer with an ALV/LSE-5004 multiple- τ
digital corrector with a 125 ns initial sampling time and a 35 mW red
HeNe linearly polarized laser operating at $\lambda = 632.8 \text{ nm}$. Nanoparticle
suspensions were loaded into 10-mm-diameter quartz cells thermo-
stated at $25 \pm 0.1^\circ\text{C}$. Data were collected using the digital ALV
correlator control software at observation angles relative to the
transmitted beam of $90/150^\circ$ (scattering vector moduli $1.87 \times 10^{-2}/$
 $2.56 \times 10^{-2} \text{ nm}^{-1}$) for a counting time of typically 180 s. In DLS
measurements, relaxation time distributions were determined using a
Contin analysis of the autocorrelation functions. Polydispersity values
were calculated from the cumulant analysis of the DLS autocorrela-
tions ($g^{(2)} - 1$).

Diffusion coefficients were obtained from eq 1 where D is the
diffusion coefficient, τ is the relaxation time, and q is the modulus of
the scattering vector:

$$D = \frac{1}{\tau q^2} \quad (1)$$

Hydrodynamic diameters, D_h , were calculated using the Stokes–
Einstein equation (eq 2), where K_B is the Boltzmann constant, T is the
temperature, η is the medium viscosity, and D is the diffusion
coefficient:

$$D_h = \frac{K_B T}{3\pi\eta D} \quad (2)$$

The percentage of small nanoparticles was calculated using eq 3, assuming that the nanoparticles behave like hard spheres in water and have the same density, where N_{small} refers to the number of small nanoparticles (fast relaxation mode), τ_{small} is the relaxation time corresponding to the small nanoparticles, and S_{small} is the surface area under the peak related to the small nanoparticles:³⁶

$$\frac{N_{\text{small}}}{N_{\text{big}}} = \left(\frac{\tau_{\text{big}}}{\tau_{\text{small}}} \right)^3 \left(\frac{S_{\text{small}}}{S_{\text{big}}} \right) \quad (3)$$

For SLS measurements, scattering intensities were corrected by the background solvent signal. The diameter of gyration, D_g , was determined from eq 4, where n is the number of repetitive units and b is the Kuhn length:

$$D_g = 2 \left(\frac{nb^2}{6} \right)^{0.5} \quad (4)$$

Electrochemistry. Electrochemical measurements were performed at room temperature using an Eco Chemie Autolab PGSTAT 100 potentiostat running GPES 4.9 software. A conventional three-electrode cell setup was used for all electrochemical experiments comprising a glassy carbon working electrode (GC, 3 mm diameter), a saturated calomel reference electrode (SCE), and a Pt wire counter electrode. The concentration of tetrazine-naphthalimide was estimated according to the Randles–Sevcik equation (eq 5) where I_p is the peak current, n is the number of electrons transferred in the redox event, F is the Faraday constant, C is the concentration of electroactive species, D is the diffusion coefficient (here estimated from dynamic light scattering), A is the geometric electrode area, ν is the scan rate, R is the gas constant, and T is room temperature:

$$I_p = nFAC \left(\frac{nF\nu D}{RT} \right)^{0.5} \quad (5)$$

Nanoparticle Tracking Analysis (NTA). NTA was carried out using a Nanosight LM10HS optical microscope setup equipped with a blue-purple laser ($\lambda_{\text{ex}} = 405 \text{ nm}$), a camera, and a chamber mounted on a modified microscope stage (Nanosight, Amesbury, U.K.). The original suspensions of nanoparticles were diluted with Milli-Q water and introduced into the chamber with a syringe. Video clips of the nanoparticles subjected to their natural Brownian motion were captured over 60 s at 25.0 °C and analyzed using analytical software version 2.1, giving access to the number-weighted size distributions. (See the Supporting Information for 10 s video clips.)

Atomic Force Microscopy (AFM). Twenty microliters of a nanoparticle suspension was dropped onto a Si(100) substrate, and the sample was left to dry at room temperature overnight in a desiccator. AFM measurements were performed using a Dimension Icon (Bruker, Santa Barbara, CA) with SCANASIST-Air (Bruker, Santa Barbara, CA) probes in peak-force mode with a scan rate of 1 Hz. The data was processed using Gwyddion 2.41 microscope software.

Fluorescence Microscopy. Twenty microliters of a nanoparticle suspension was dropped onto a Si(100) substrate, and the sample was left to dry at room temperature overnight in a desiccator. Fluorescence microscopy images were recorded using an Olympus BX61 microscope coupled with an Olympus DP30BW camera and CellP imaging software. A DAPI (4',6-diamidino-2-phenylindole) filter set was used: DAPI with $\lambda_{\text{ex}} = 340\text{--}380 \text{ nm}$ and $\lambda_{\text{em}} = 450\text{--}490 \text{ nm}$. Images were recorded with an exposure time of 500 ms.

RESULTS AND DISCUSSION

For the preparation of nanoparticles in aqueous solution via nanoprecipitation, we focused our initial studies on optimizing the solvent system for both blocks of the PS-CD glycopolymer. Tetrahydrofuran was chosen as the organic solvent because of its good solubility toward polystyrenes and Tz, water miscibility, and good evaporation rate. Static light scattering

experiments were recorded for a series of PS-CD solutions prepared in THF with water content of between 0 and 50% (Figure S2). Very low scattering intensities were observed in the presence of 5 to 20% water, consistent with desirable polymer chain dissolution and few aggregates in a mixed solvent. In the presence of $\geq 20\%$ water, a significant increase in scattering intensity was observed because of the unwanted formation of self-assemblies. β -Cyclodextrin-modified polymer solutions were therefore investigated in 10 and 20% water solutions. However, further observations proved that suspensions based on 10% water solutions were more unstable, with microscopic particles visible after just a few days of storage, and thus the 80:20 THF/water ratio was adopted for further investigations.

We explored the controlled self-assembly of PS-CD (1 mg g^{-1}) in the presence and absence of Tz (0.2 mg g^{-1}) in THF/H₂O via nanoprecipitation in a large excess of water (Figure 1A). For the PS-CD with Tz solution, the PS-CD/Tz mole-to-

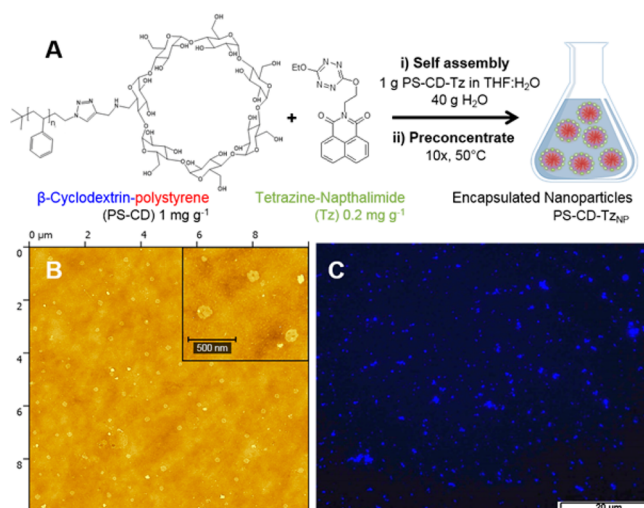


Figure 1. (A) Synthesis route for the preparation of encapsulated nanoparticles (PS-CD-Tz_{NP}). (B, C) Images of PS-CD-Tz_{NP} particles prepared by method A on silicon recorded by (B) AFM in peak-force mode at 1 Hz and (C) fluorescence microscopy with a DAPI filter and a 500 ms exposure time.

mole ratio used was 1:3. Herein, suspensions obtained from PS-CD and PS-CD with Tz will be referred to as PS-CD_{NP} and PS-CD-Tz_{NP}, respectively. Two methods of nanoprecipitation were explored: method A, where 1 g of PS-CD polymer solution was slowly added to 40 g of water (solvent-to-water method), and method B, where 40 g of water was slowly added to 1 g of PS-CD polymer solution (water-to-solvent method). For both methods A and B, the same precipitation and evaporation procedures were performed (Experimental Section) to obtain aqueous PS-CD_{NP} and PS-CD-Tz_{NP} suspensions.

The ability of the β -cyclodextrin-modified polystyrene solutions to spontaneously assemble into nanoparticles was initially confirmed by atomic force microscopy and fluorescence microscopy after solution drop-casting and drying on a silicon wafer (Figure 1B,C). AFM imaging of the PS-CD-Tz_{NP} sample prepared by method A revealed the presence of individual nanoparticles with an average particle diameter of $167 \pm 30 \text{ nm}$ ($n = 89$ particles). Importantly, the brief AFM analysis proved the successful formation of nanoparticle self-assemblies using our nanoprecipitation protocol. Figure 1C shows a fluorescence

microscopy image of the PS-CD-Tz_{NP} sample recorded with a DAPI filter at $\lambda_{\text{ex}} = 340\text{--}380$ nm and $\lambda_{\text{em}} = 450\text{--}490$ nm. Bright fluorescence over a long lifetime using a DAPI filter was observed from the particles on the surface. In contrast, insignificant fluorescence was observed for PS-CD_{NP} (data not shown), consistent with the successful encapsulation of the small organic tetrazine-containing bifluorophore in PS-CD-Tz_{NP} particles.²⁸

Dynamic light scattering experiments were performed to examine the suspensions in more detail. Initial DLS was performed on PS-CD_{NP} (Figure 2A) and PS-CD-Tz_{NP} (Figure 2B) prepared by methods A and B to optimize the nanoprecipitation protocol for the preparation of well-defined nanoassemblies.

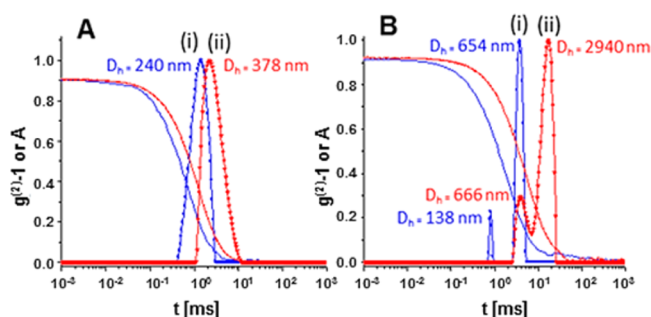


Figure 2. DLS autocorrelation ($g^{(2)} - 1$) measured at 90° and relaxation time distribution of aqueous suspensions of (A) PS-CD_{NP} prepared by (i) method A and (ii) method B and (B) PS-CD-Tz_{NP} prepared by (i) method A and (ii) method B.

Figure 2A shows the DLS autocorrelation function ($g^{(2)} - 1$) and relaxation time distribution for the PS-CD_{NP} suspensions. For PS-CD_{NP} prepared by methods A (Figure 2Ai) and B (Figure 2Aii), unimodal distributions of relaxation times were observed corresponding to mean hydrodynamic diameters of $D_h = 240$ and 378 nm with polydispersities of $\mathcal{D} = 1.34$ and 1.45 , respectively. The particles prepared by method A are therefore smaller and less polydisperse than those prepared by method B. The PS-CD_{NP} particles prepared by method A are comparable in size to previously reported compound micelles with $D_h \approx 160$ nm prepared by the self-assembly of polystyrene-containing diblock polymers.^{10,15} Figure 2B shows the DLS autocorrelation function ($g^{(2)} - 1$) and relaxation time distribution for the PS-CD-Tz_{NP} suspensions prepared by methods A (Figure 2Bi) and B (Figure 2Bii). The relaxation time distribution plots, reflecting mass-weighted distributions, show the appearance of two particle sizes for PS-CD-Tz_{NP}. The PS-CD-Tz_{NP} suspension obtained by method B exhibits greater polydispersity ($\mathcal{D} = 1.43$) and contains microscale particles ($D_h = 2940$ nm). In contrast, smaller nanoparticles with a lower polydispersity ($\mathcal{D} = 1.32$) are obtained by method A, and thus this method of nanoprecipitation was adopted for further analysis.

The smaller particle size of $D_h = 138$ nm observed for PS-CD-Tz_{NP} prepared by method A is attributed to small self-assemblies that have decreased in size compared to the PS-CD_{NP} nanoparticles prepared by the same method as a result of the encapsulation of Tz molecules and the shrinking of the more hydrophobic core. A change in self-assembly behavior of the PS-CD polymer in the presence of Tz was expected because the cone-shaped hydrophobic cavities of the β -cyclodextrin groups drive the 1:1 inclusion of guest Tz molecules via 1,8-

naphthalimide (equatorial inclusion) and 1,2,4,5-tetrazine 336 groups.^{29,37} A decrease in size with encapsulation has previously 337 been reported for self-assembled nanoparticles with encapsu- 338 lated hydrophobic molecules.¹⁵ The larger nanoparticles of PS- 339 CD-Tz_{NP} with $D_h = 654$ nm, observed only after self-assembly 340 in the presence of Tz, are attributed to nanoparticle clusters. 341 The formation of clusters is attributed to the cross-linking of 342 individual particles via host–guest interactions between Tz 343 molecules and host β -cyclodextrin groups located at the 344 periphery of the particles. (Both tetrazine and naphthalimide 345 functional groups can function as guests.) Particle aggregation 346 due to nonspecific interactions³ must be considered and likely 347 contributes to the self-assembly of the larger particle 348 distribution. Regardless of the nature of formation of the larger 349 particles, their presence in terms of number is very small 350 compared to the smaller particles. On the basis of 12 DLS 351 measurements at 90° , the estimated number of smaller objects 352 is 95.1% ($N_{\text{small}} \approx 19.1N_{\text{big}}$), according to eq 3. 353

To complete the nanoparticle sizing experiments, nano- 354 particle tracking analysis was performed. Nanoparticles were 355 illuminated with a 405 nm blue laser and tracked individually 356 (Figure 3, Figure S3 and corresponding video clips in the 357

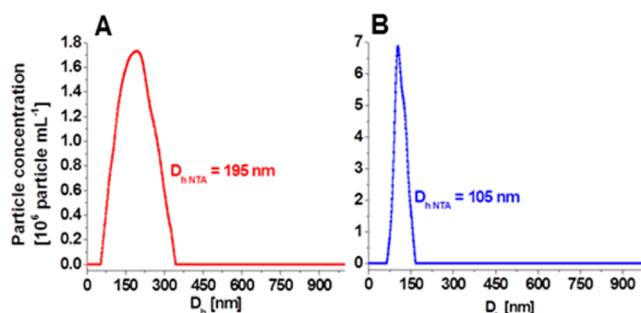


Figure 3. Hydrodynamic number-weighted size distributions by NTA of (A) PS-CD_{NP} and (B) PS-CD-Tz_{NP} suspensions prepared by method A.

Supporting Information). Nanoparticles that undergo Brownian 358 motion were taken into account, and average $D_{h,\text{NTA}}$ values of 359 195 nm for PS-CD_{NP} and 105 nm for PS-CD-Tz_{NP} were 360 acquired. These values are smaller than those obtained by DLS 361 because of the fact that number-weighted distributions are 362 obtained. Nevertheless, the sizes obtained by NTA are 363 complementary, with the corresponding particle sizes obtained 364 by DLS ($D_h = 240$ and 138 nm). The absence of the larger 365 cluster distribution for PS-CD-Tz_{NP} by NTA is not at all 366 surprising given that (i) NTA gives access to number-weighted 367 distributions of which only $\sim 4.9\%$ are the clusters and (ii) only 368 a few nanoparticles are imaged, as can be seen in Figure S3 and 369 the video clips. 370

Further analysis of the DLS and SLS scattering data was 371 performed to shed light on the shape of the nanoparticles. First, 372 the diameter of gyration, D_g , was determined from SLS angular 373 dependence experiments via Guinier plots (Figure 4). Values of 374 $D_g = 326$ and 258 nm were obtained from the slope of the 375 linear fit in the low qD_g region for PS-CD_{NP} and PS-CD-Tz_{NP}, 376 respectively. Next, the shape factor, ρ , was obtained from the 377 ratio $\rho = D_g/D_h$, as proposed by Burchard.³⁸ The ρ values of 1.4 378 for PS-CD_{NP} and 1.9 for PS-CD-Tz_{NP} fall between those of 379 vesicles ($\rho = 1$) and rigid rods ($\rho \geq 2.0$), and thus PS-CD_{NP} 380 and PS-CD-Tz_{NP} particles can be ascribed to particles whose 381

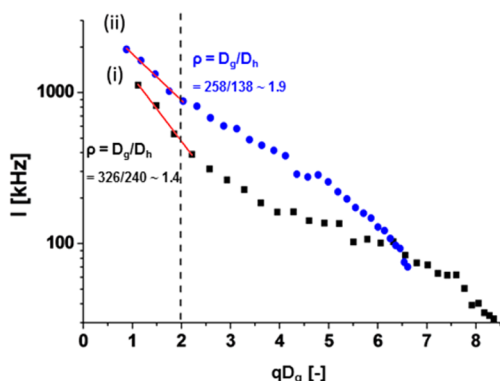


Figure 4. SLS Guinier plots of the scattering intensity of (i) PS-CD_{NP} and (ii) PS-CD-Tz_{NP} suspensions prepared by method A.

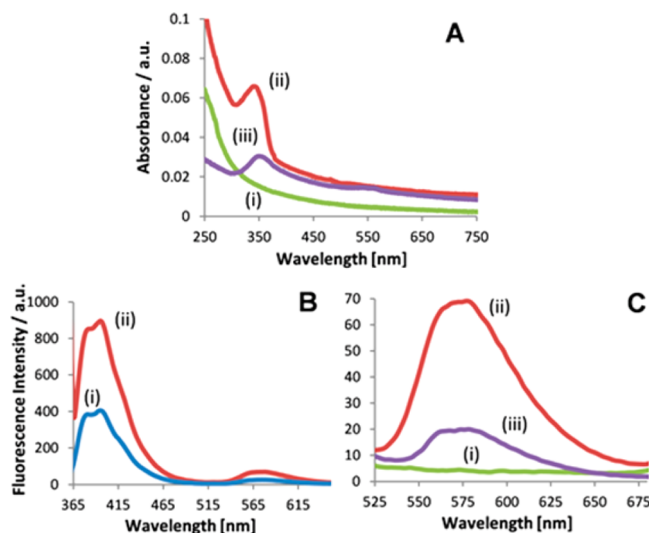


Figure 5. (A) UV-vis absorption spectra for (i) PS-CD_{NP}, (ii) PS-CD-Tz_{NP}, and (iii) H₂O-Tz. (B, C) Fluorescence emission spectra recorded at $\lambda_{\text{ex}} = 353$ nm for (B) PS-CD-Tz_{NP} at 365 to 650 nm and (C) (i) PS-CD_{NP}, (ii) PS-CD-Tz_{NP}, and (iii) H₂O-Tz at 525 to 680 nm.

blocked as a consequence of the encapsulation process. This is in sharp contrast to the situation encountered when the molecules are dissolved in an organic solvent, where the energy transfer occurs with a ca. 90% efficiency and only tetrazine fluorescence is observed.²⁸

Fluorescence spectra of PS-CD-Tz_{NP} nanoparticles were initially recorded at different emission wavelengths. Strong fluorescence was observed only upon excitation in the UV region at $\lambda_{\text{ex}} = 353$ nm (Figure 5B) and $\lambda_{\text{ex}} = 340$ nm (data not shown) and not at higher wavelengths (for example, $\lambda_{\text{ex}} = 518$ and 544 nm, data not shown). The classical strong fluorescence of 1,8-naphthalimide was observed between 370 and 420 nm along with a weak fluorescence band at 550–600 nm due to the tetrazine moiety. Further evidence for the improved uptake of fluorescent Tz molecules via molecular encapsulation was obtained by comparison of the fluorescence spectra recorded at $\lambda_{\text{ex}} = 340$ nm for PS-CD_{NP}, PS-CD-Tz_{NP}, and H₂O-Tz solutions (Figure 5C). No fluorescence was observed for nanoparticles free of Tz (Figure 5Ci), as expected. A clear enhancement in fluorescence was, however, observed at $\lambda_{\text{em}} = 570$ nm for PS-CD-Tz_{NP} (Figure 5Cii) compared to the Tz-saturated H₂O-Tz solution, reflecting the improved solubility of tetrazine-naphthalimide in the nanoparticle solution compared to water.

Cyclic voltammograms (CVs) of the solutions were also performed to test the electroactivity of the nanoparticles. CVs were recorded at glassy carbon electrodes without supporting electrolyte to avoid aggregation due to increased ionic strength. In the absence of Tz, a typical background response of a GC electrode in aqueous solution was observed (Figure 6Ai). For PS-CD-Tz_{NP} nanoparticles, a single well-defined and chemically reversible redox couple at $E_{1/2} = -0.32$ V vs SCE was observed (Figure 6Aii). This system is attributed to a two-electron, two-proton reduction of 1,4-tetrazine to its protonated form, 1,4-dihydropyridazine.^{29,39} This behavior is analogous to the two-electron reduction of quinones to hydroquinones in aqueous solution. It should be noted that the CV recorded in H₂O-Tz solution (Figure 6Si) shows an almost identical $E_{1/2}$ but with an extremely weak peak intensity, reflecting the trace presence of

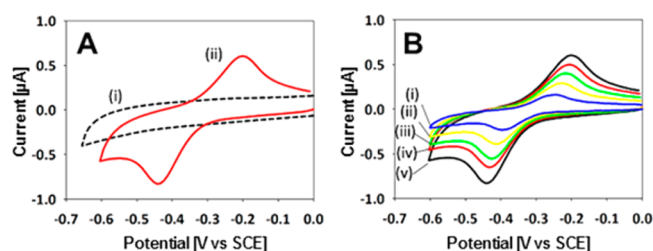


Figure 6. CVs recorded at glassy carbon on (A) (i) PS-CD_{NP} and (ii) PS-CD-Tz_{NP} at 100 mV s⁻¹ and (B) PS-CD-Tz_{NP} at (i) 20, (ii) 40, (iii) 60, (iv) 80, and (v) 100 mV s⁻¹.

Tz for the Tz-saturated H₂O solution. However, the peak-to-peak separation for H₂O-Tz ($\Delta E_p = 149$ mV) is smaller than that recorded for PS-CD-Tz_{NP}, suggesting slower apparent electron-transfer kinetics for the encapsulated nanoparticles. The latter may be assigned to a phenomenon of electron hopping between Tz molecules encapsulated within cyclodextrin groups located at the periphery and inside the poorly conducting polystyrene core. Thus, the tetrazine-containing nanoparticles are redox-active and electrochemically accessible, which has important implications for future catalytic and sensing applications.

Finally, CVs of the PS-CD-Tz_{NP} solution were recorded at scan rates in the range of 20 to 100 mV s⁻¹. A linear dependence between the peak current and the square root of the scan rate, indicative of diffusion-controlled behavior (Figure S6), was observed. Assuming diffusion-controlled behavior, we applied the Randles–Sevcik equation (eq 5) to estimate the average concentration of electroactive Tz molecules encapsulated in the nanoparticles, thus providing an idea of possible drug or redox molecule loading capacity. From the oxidative peak current shown in Figure 6A and using the diffusion coefficient obtained for the small particles of 3.57×10^{-8} cm² s⁻¹ via DLS analysis using eq 1, the estimated Tz concentration for PS-CD-Tz_{NP} is 1.5×10^{-4} mol L⁻¹.

CONCLUSIONS

A new bioinspired β -cyclodextrin-modified polystyrene polymer has been prepared using a heterogeneous copper nanocatalyst that facilitates glycopolymer purification and preparation on a larger scale. Self-assembly via a “solvent-to-water” nanoprecipitation method, in the presence of tetrazine-naphthalimide, forms stable redox-active nanoassembled particles and clusters with mean hydrodynamic diameters of 138 and 654 nm, respectively. The nanoparticles are considered to be spheres constituting β -cyclodextrin and polystyrene blocks, with β -cyclodextrin groups present in the outer layer. Increased UV absorption, fluorescence, and electrochemical signals confirm both the presence and improved uptake of tetrazine-naphthalimide molecules in nanoparticles compared to water. Solvchromatic shifts and a slight decrease in electrochemical reversibility for the redox-active molecules in the nanoparticles are consistent with their encapsulation in the nanoparticles and their surface via Tz inclusion in β -cyclodextrin groups. Furthermore, the fluorescence emission reveals that both the imide antenna and tetrazine acceptor emit together, proving that the energy transfer between the chromophores is partially deactivated. As a consequence, the fluorescence emission is less brilliant than that observed for the tetrazine-naphthalimide dyad in organic solvent. The formation of a small number of large clusters, observed here only by light

scattering experiments, is possible via a novel type of host–guest interparticle cross-linking where tetrazine-naphthalimide molecules act as a nanoparticle cross-linker. The potential use of the new glycopolymer for host–guest encapsulation of electrocatalysts for the construction of enzymatic biofuel cells with improved performance and biocompatibility is currently underway.

ASSOCIATED CONTENT

Supporting Information

The Supporting Information is available free of charge on the ACS Publications website at DOI: 10.1021/acs.langmuir.6b03512.

Glycopolymer synthesis details and characterization data by DLS, NTA, and voltammetry (PDF)

Nanoparticle tracking analysis of PS-CD and PS-CD-Tz_{NP} suspensions prepared by method A (ZIP)

AUTHOR INFORMATION

Corresponding Authors

*E-mail: borsali@cervav.cnrs.fr.

*E-mail: serge.cosnier@univ-grenoble-alpes.fr.

Notes

The authors declare no competing financial interest.

ACKNOWLEDGMENTS

This work was supported by LABEX ARCANÉ (ANR-11-LABX-0003-01) and platform Chimie NanoBio ICMG FR 2607 (PCN-ICMG). We gratefully acknowledge the assistance of Hugues Bonnet with AFM imaging.

REFERENCES

- Gaitzsch, J.; Huang, X.; Voit, B. Engineering Functional Polymer Capsules toward Smart Nanoreactors. *Chem. Rev.* **2016**, *116* (3), 1053–1093.
- Nicolas, J.; Mura, S.; Brambilla, D.; Mackiewicz, N.; Couvreur, P. Design, Functionalization Strategies and Biomedical Applications of Targeted Biodegradable/Biocompatible Polymer-Based Nanocarriers for Drug Delivery. *Chem. Soc. Rev.* **2013**, *42* (3), 1147–1235.
- Qu, X.; Khutoryanskiy, V. V.; Stewart, A.; Rahman, S.; Papahadjopoulos-Sternberg, B.; Dufes, C.; McCarthy, D.; Wilson, C. G.; Lyons, R.; Carter, K. C.; Schatzlein, A.; Uchegbu, I. F. Carbohydrate-Based Micelle Clusters which Enhance Hydrophobic Drug Bioavailability by up to 1 Order of Magnitude. *Biomacromolecules* **2006**, *7* (12), 3452–3459.
- Li, C. H.; Liu, S. Y. Polymeric Assemblies and Nanoparticles with Stimuli-Responsive Fluorescence Emission Characteristics. *Chem. Commun.* **2012**, *48* (27), 3262–3278.
- Farokhzad, O. C.; Cheng, J. J.; Tepley, B. A.; Sherifi, I.; Jon, S.; Kantoff, P. W.; Richie, J. P.; Langer, R. Targeted Nanoparticle-Aptamer Bioconjugates for Cancer Chemotherapy in vivo. *Proc. Natl. Acad. Sci. U. S. A.* **2006**, *103* (16), 6315–6320.
- Meier, W. Polymer Nanocapsules. *Chem. Soc. Rev.* **2000**, *29* (5), 295–303.
- Xu, Z.; Liu, S.; Liu, H.; Yang, C.; Kang, Y.; Wang, M. Unimolecular Micelles of Amphiphilic Cyclodextrin-Core Star-like Block Copolymers for Anticancer Drug Delivery. *Chem. Commun.* **2015**, *51* (87), 15768–15771.
- Zhang, Y.; Hsu, B. Y. W.; Ren, C. L.; Li, X.; Wang, J. Silica-Based Nanocapsules: Synthesis, Structure Control and Biomedical Applications. *Chem. Soc. Rev.* **2015**, *44* (1), 315–335.
- Kakuchi, T.; Narumi, A.; Miura, Y.; Matsuya, S.; Sugimoto, N.; Satoh, T.; Kaga, H. Glycoconjugated Polymer. 4. Synthesis and Aggregation Property of Well-Defined End-Functionalized Polystyrene with β -Cyclodextrin. *Macromolecules* **2003**, *36* (11), 3909–3913.

- (10) Otsuka, I.; Osaka, M.; Sakai, Y.; Travelet, C.; Putaux, J.-L.; Borsali, R. Self-Assembly of Maltoheptaose-block-Polystyrene into Micellar Nanoparticles and Encapsulation of Gold Nanoparticles. *Langmuir* **2013**, *29* (49), 15224–15230.
- (11) Houga, C.; Le Meins, J. F.; Borsali, R.; Taton, D.; Gnanou, Y. Synthesis of ATRP-Induced Dextran-b-Polystyrene Diblock Copolymers and Preliminary Investigation of their Self-Assembly in Water. *Chem. Commun.* **2007**, *29*, 3063–3065.
- (12) Ouhib, R.; Renault, B.; Mouaziz, H.; Nouvel, C.; Dellacherie, E.; Six, J. L. Biodegradable Amylose-g-PLA Glycopolymers from Renewable Resources. *Carbohydr. Polym.* **2012**, *89* (1), 305–305.
- (13) Giacomelli, C.; Schmidt, V.; Putaux, J. L.; Narumi, A.; Kakuchi, T.; Borsali, R. Aqueous Self-Assembly of Polystyrene Chains End-Functionalized with beta-Cyclodextrin. *Biomacromolecules* **2009**, *10* (2), 449–453.
- (14) Suriano, F.; Coulembier, O.; Degee, P.; Dubois, P. Carbohydrate-based amphiphilic diblock copolymers: Synthesis, Characterization, and Aqueous Properties. *J. Polym. Sci., Part A: Polym. Chem.* **2008**, *46* (11), 3662–3672.
- (15) He, Q.; Wu, W.; Xiu, K.; Zhang, Q.; Xu, F.; Li, J. Controlled Drug Release System Based on Cyclodextrin-Conjugated Poly(lactic acid)-b-Poly(ethylene glycol) Micelles. *Int. J. Pharm.* **2013**, *443* (1–2), 110–119.
- (16) Zepon, K.; Otsuka, I.; Bouilhac, C.; Muniz, E. C.; Soldi, V.; Borsali, R. Self-assembly of Oligosaccharide-b-PMMA Block Copolymer Systems: Glyco-Nanoparticles and their Degradation under UV Exposure. *Langmuir* **2016**, *32* (18), 4538–4545.
- (17) Cianga, L.; Bendrea, A.-D.; Fifere, N.; Nita, L. E.; Doroftei, F.; Ag, D.; Selec, M.; Timur, S.; Cianga, I. Fluorescent Micellar Nanoparticles by Self-Assembly of Amphiphilic, Nonionic and Water Self-Dispersible Polythiophenes with "Hairy Rod" Architecture. *RSC Adv.* **2014**, *4* (99), 56385–56405.
- (18) Xu, B.; Gu, G.; Feng, C.; Jiang, X.; Hu, J.; Lu, G.; Zhang, S.; Huang, X. (PAA-g-PS)-co-PPEGMEMA Asymmetric Polymer Brushes: Synthesis, Self-Assembly, and Encapsulating Capacity for both Hydrophobic and Hydrophilic Agents. *Polym. Chem.* **2016**, *7* (3), 613–624.
- (19) Yin, L.; Dalsin, M. C.; Sizovs, A.; Reineke, T. M.; Hillmyer, M. A. Glucose-Functionalized, Serum-Stable Polymeric Micelles from the Combination of Anionic and RAFT Polymerizations. *Macromolecules* **2012**, *45* (10), 4322–4332.
- (20) Fessi, H.; Devissaguet, J. P.; Puisieux, F.; Thies, C. Method of Formation of Colloidal Nanoparticles. FR 2,608,988 A1 1988.
- (21) Fessi, H.; Puisieux, F.; Devissaguet, J. P.; Ammouy, N.; Benita, S. Nanocapsule Formation by Interfacial Polymer Deposition following Solvent Displacement. *Int. J. Pharm.* **1989**, *55* (1), R1–R4.
- (22) Zepon, K. M.; Otsuka, I.; Bouilhac, C.; Muniz, E. C.; Soldi, V.; Borsali, R. Glyco-Nanoparticles Made from Self-Assembly of Maltoheptaose-block-Poly(methyl methacrylate): Micelle, Reverse Micelle, and Encapsulation. *Biomacromolecules* **2015**, *16* (7), 1212–1224.
- (23) McLaughlin, C. K.; Logie, J.; Shoichet, M. S. Core and Corona Modifications for the Design of Polymeric Micelle Drug-Delivery Systems. *Isr. J. Chem.* **2013**, *53* (9–10), 670–679.
- (24) Kang, Y.; Guo, K.; Li, B. J.; Zhang, S. Nanoassemblies Driven by Cyclodextrin-Based Inclusion Complexation. *Chem. Commun.* **2014**, *50* (76), 11083–11092.
- (25) Stoffelen, C.; Huskens, J. Soft Supramolecular Nanoparticles by Noncovalent and Host-Guest Interactions. *Small* **2016**, *12* (1), 96–119.
- (26) Guo, M.; Jiang, M.; Zhang, G. Surface Modification of Polymeric Vesicles via Host-Guest Inclusion Complexation. *Langmuir* **2008**, *24* (19), 10583–10586.
- (27) Versluis, F.; Tomatsu, I.; Kehr, S.; Fregonese, C.; Tepper, A. W. J. W.; Stuart, M. C. A.; Ravoo, J.; Koning, R.; Kros, A. Shape and Release Control of a Peptide Decorated Vesicle through pH Sensitive Orthogonal Supramolecular Interactions. *J. Am. Chem. Soc.* **2009**, *131* (37), 13186–13187.
- (28) Zhou, Q.; Audebert, P.; Clavier, G.; Meallet-Renault, R.; Miomandre, F.; Shaukat, Z.; Vu, T. T.; Tang, J. New Tetrazines Functionalized with Electrochemically and Optically Active Groups: Electrochemical and Photoluminescence Properties. *J. Phys. Chem. C* **2011**, *115* (44), 21899–21906.
- (29) Fritea, L.; Audebert, P.; Galmiche, L.; Gorgy, K.; Le Goff, A.; Villalonga, R.; Săndulescu, R.; Cosnier, S. First Occurrence of Tetrazines in Aqueous Solution: Electrochemistry and Fluorescence. *ChemPhysChem* **2015**, *16* (17), 3695–3699.
- (30) Fulmer, G. R.; Miller, A. J. M.; Sherden, N. H.; Gottlieb, H. E.; Nudelman, A.; Stoltz, B. M.; Bercaw, J. E.; Goldberg, K. I. NMR Chemical Shifts of Trace Impurities: Common Laboratory Solvents, Organics, and Gases in Deuterated Solvents Relevant to the Organometallic Chemist. *Organometallics* **2010**, *29* (9), 2176–2179.
- (31) Fallais, I.; Devaux, J.; Jérôme, R. End-Capping of Polystyrene by Aliphatic Primary Amine by Derivatization of Precursor Hydroxyl End Group. *J. Polym. Sci., Part A: Polym. Chem.* **2000**, *38* (9), 1618–1629.
- (32) Moutard, S.; Relation entre la Structure et les Propriétés d'Organisation de Nouvelles Cyclodextrines Amphiphiles. Ph.D. Thesis, Picardie Jules Verne University, France, 2003.
- (33) Guo, Z.; Jin, Y.; Liang, T.; Liu, Y.; Xu, Q.; Liang, X.; Lei, A. Synthesis, Chromatographic Evaluation and Hydrophilic Interaction/Reversed-Phase Mixed-Mode Behavior of a "Click β -Cyclodextrin" Stationary Phase. *J. Chromatogr. A* **2009**, *1216* (2), 257–263.
- (34) Elamari, H.; Etudes sur la Catalyse de la Reaction de Huisgen et Nouvelles Applications Synthétiques. Ph.D. Thesis, University Pierre and Marie Curie, France, 2013.
- (35) Isaacman, M. J.; Barron, K. A.; Theogarajan, L. S. Clickable Amphiphilic Triblock Copolymers. *J. Polym. Sci., Part A: Polym. Chem.* **2012**, *50* (12), 2319–2329.
- (36) Korchia, L.; Bouilhac, C.; Lapinte, V.; Travelet, C.; Borsali, R.; Robin, J.-J. Photodimerization as an Alternative to Photocrosslinking of Nanoparticles: Proof of Concept with Amphiphilic Linear Polyoxazoline Bearing Coumarin Unit. *Polym. Chem.* **2015**, *6* (33), 6029–6039.
- (37) Brochsztain, S.; Rodrigues, M. A.; Politi, M. J. Inclusion Complexes of Naphthalimide Derivatives with Cyclodextrins. *J. Photochem. Photobiol., A* **1997**, *107* (1–3), 195–200.
- (38) Walther, B. In *Polysaccharides: Structural Diversity and Functional Versatility*; Dumitriu, S., Ed.; CRC Press: New York, 2004; Chapter 7.
- (39) Ehret, F.; Wu, H. X.; Alexander, S. C.; Devaraj, N. K. Electrochemical Control of Rapid Bioorthogonal Tetrazine Ligations for Selective Functionalization of Microelectrodes. *J. Am. Chem. Soc.* **2015**, *137* (28), 8876–8879.